Available online at www.sciencedirect.com

ScienceDirect

IFAC Papers Online CONFERENCE PAPER ARCHIVE

IFAC PapersOnLine 50-1 (2017) 3977–3982

Robust Autopilot Design for Crosswind Landing

Julian Theis * **Daniel Ossmann** ** **Harald Pfifer** ***

* *Institute of Control Systems, Hamburg University of Technology, Hamburg, Germany (e-mail: julian.theis@tuhh.de.)*

** *Aerospace Engineering and Mechanics Department, University of Minnesota, Minneapolis, MN, USA (e-mail: dossmann@umn.edu)*

*** *Mechanical Engineering Department, University of Nottingham, Nottingham, UK (e-mail: harald.pfifer@nottingham.ac.uk)*

Abstract: A comprehensive autolanding design for the representative model of a twin-engined commercial aircraft is presented in this paper. A cascaded structure is selected to facilitate the design task and to minimize control law switching. Classical loopshaping and robust control techniques are used to design the individual control loops. The emphasis is on design parameters with a clear relation to design objectives, resulting in an intuitive tuning procedure. The control system's ability to safely land the aircraft despite strong crosswind in a variety of possible scenarios is demonstrated in an industry-grade verification campaign. Monte Carlo simulations are used to assess the risk of unsafe landing conditions and provide insight into the performance characteristics and limitations of the proposed control system.

Keywords: Flight control, Robust control applications

1. INTRODUCTION

Automatic control systems play a fundamental role in modern civil aviation and are by now capable of assisting the pilot in all flight segments. In fact, today's autopilots autonomously perform challenging maneuvers such as landing the aircraft in poor visibility. To safely land the aircraft, the autopilot has to achieve a very high level of precision in a variety of scenarios. Especially crosswind poses a severe danger to landing aircraft. The autolanding system of the A320, e. g. is only certified to perform safe landings in crosswind up to 20 knots. For comparison, the demonstrated crosswind in manual flight operation (that requires clear sight of the runway) on the A320 is 35 knots. Improving the ability of autolanding systems to handle adverse wind conditions is thus important to increase performance, reliability, safety, and comfort of future civilian aircraft. Consequently, several researchers have investigated the potential of modern control techniques for this application, e. g., Holley and Bryson (1977); Looye et al. (2001); de Bruin and Jones (2016)

This paper is in response to a design challenge proposed by ONERA and AIRBUS in Biannic and Boada-Bauxell (2016) and based on the aircraft model introduced in Biannic and Roos (2015). The goal is to design an autolanding system for the representative model of a twin-engined commercial transport aircraft in (full) landing configuration that maximizes allowable crosswind. Requirements are quantified by risk dispersions and are evaluated through Monte Carlo simulations over a wide range of environmental and system parameters. Dispersions for the risk of short landing, long landing, hard landing, decentered landing, as well as landing with steep bank angle and landing with steep wheel sideslip angle must be satisfied. In short, the autopilot must steer the aircraft through the final approach starting 300 m above the runway all the way to touchdown. Success is defined as a gentle touchdown close to the runway centerline with wings level and landing gear aligned with the runway. Available data to perform this task is based on current CAT-III instrument landing systems (ILS) and includes measurements of both vertical and horizontal deviation from the glide path. This paper develops an autopilot that satisfies the performance criteria for up to 25 knots crosswind. A cascaded control structure is proposed in Section 2. The design uses classical loopshaping and H_∞ control, and is therefore very comprehensible, see Section 3. The focus is on the choice of design parameters with a clear relation to the design objectives, see Section 4. The design is evaluated in Section 5 through Monte Carlo simulations, verifying robust performance.

2. AUTOMATED LANDING CONTROL PROBLEM

The aircraft considered in this paper is described by a standard six-degrees-of-freedom flight mechanics model (e. g. McRuer et al., 1973; Brockhaus et al., 2013) in terms of translational velocities u, v, w and angular velocities p (roll), q (pitch), r (yaw) in the body-fixed frame. Orientation in the earth-fixed reference frame is described in terms of Euler angles Φ (bank), Θ (pitch), and Ψ (heading). The angles between body-fixed frame and wind axis are angle of attack α and sideslip angle β. The flight path is described with respect to earth by path angle γ, course angle χ, and ground speed V_g. Its orientation differs from the wind axis by the angles α_W and β_W with the approximate relation (Brockhaus et al., 2013)

$$\begin{bmatrix}\beta\\ \alpha\end{bmatrix} + \begin{bmatrix}\beta_W\\ \alpha_W\end{bmatrix} = \begin{bmatrix}\cos(\Phi) & \sin(\Phi)\\ -\sin(\Phi) & \cos(\Phi)\end{bmatrix} \begin{bmatrix}\chi - \Psi\\ \Theta - \gamma\end{bmatrix}. \quad (1)$$

10.1016/j.ifacol.2017.08.770

In the first segment of the final approach, the aircraft must track a given glide path both in vertical and horizontal direction. This requires not only to maintain γ and χ, but also to counteract wind that drives the aircraft away from the glide path. The deviation in vertical (Δz) and horizontal (Δy) direction hence must be controlled to zero. These deviations are available from the ILS. Once the aircraft is close to the ground, sink rate is reduced for touchdown in a maneuver called "flare". The aircraft is further aligned with the direction of the runway in a maneuver called "decrab", and the wings are leveled before touchdown to prevent the danger of touching the ground. Throttle (δ_{th}) and elevator (δ_{e}) are the available actuators for longitudinal control. Lateral-directional control uses ailerons (δ_{a}) and rudder (δ_{r}). To facilitate the design task, a series of cascaded control systems, illustrated in Fig. 1, is developed. This requires to keep consecutive loops apart by a factor of two in frequency with the ultimate constraints being the servo actuator bandwidths.

2.1 Longitudinal Control Architecture

Throttle and elevator bandwidths differ considerably (0.5 rad/s to 14 rad/s) such that a combined control design does not promise any advantages. The setpoint V_{ref} for the calibrated airspeed V_{cas} is constant and it is decided to solely use throttle to control airspeed. This autothrottle is constrained by the engine control bandwidth to less than 0.25 rad/s. A pitch rate tracker is used as the basis for longitudinal control. The control loop bandwidth is limited by the servo actuator to less than 7 rad/s. The pitch rate tracker augments the short period dynamics and acts as an attitude hold controller in steady flight.

The first outer loop is a sink rate (V_z) tracker that is used both during approach and flare. During flare, the objective is to directly control V_z. During approach, a glide path defined by a constant flight path angle $\gamma \approx {}^{V_z}/_{V_{\mathrm{g}}}$ needs to be tracked. Controlling V_z is essentially the same as controlling γ since $V_{\mathrm{g}} \gg V_z$ and the relative influence of gusts on the ground speed is much lower than on the sink rate. Hence, the same controller can be used for both flight phases. The sink rate loop is constrained not only by the pitch control bandwidth, but also by a non-minimum phase zero with a frequency of about 2.5 rad/s. This zero is associated with the acceleration response to elevator deflection. Maintaining also a factor of two with respect to this frequency yields a bandwidth limit of 1.25 rad/s.

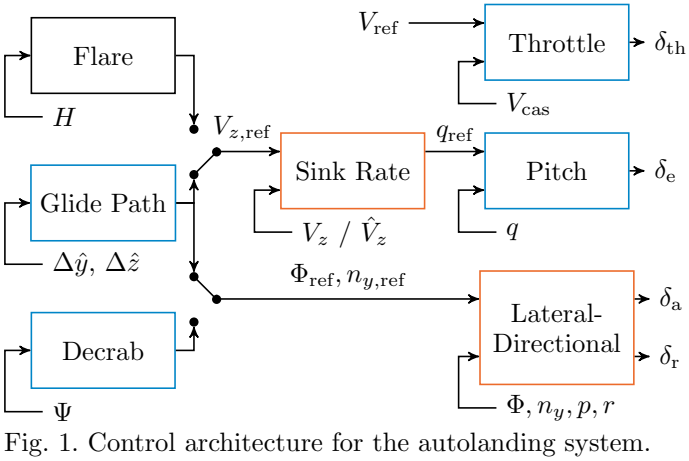

Fig. 1. Control architecture for the autolanding system.

Control laws are switched for approach and flare only in the second outer loop. During approach, the reference sink rate is generated by feeding back the vertical deviation Δz to keep the aircraft on the glide path. During flare, the height above the runway H is fed back to generate a reference sink rate that vertically decelerates the aircraft for touchdown. Both of these loops are limited by the sink rate control loop and must be slower than about 0.6 rad/s.

2.2 Lateral-Directional Control Architecture

The available servo actuator bandwidths are 16 rad/s for ailerons and 5 rad/s for rudder. The lateral directional control problem is necessarily multivariable and requires the coordinated use of ailerons and rudder. Control design thus has to acknowledge these different bandwidths. The standard paradigm for landing in crosswind is the "crabbed approach": The aircraft is held level ($\Phi = 0$) and the sideslip angle β is controlled to zero which according to (1) yields $\Psi \approx -\beta_W$, i. e., the aircraft's nose is pointed into the wind. Following this paradigm, it is decided to track the bank angle Φ and the lateral acceleration n_y (as a surrogate for β). The bank angle reference during approach is provided by feeding back the vertical deviation Δy to keep the aircraft on the glide path ($\chi = 0$). The reference for n_y is zero during approach. To decrab before touchdown, Ψ is fed back to generate an n_y reference until the aircraft is aligned with the runway and Φ is commanded to zero in order to level the wings. Roll rate p and yaw rate r are also fed back as auxiliary signals to improve the lightly damped dutch roll dynamics.

2.3 Signal Modifications

The deviations Δz and Δy are obtained from the ILS glide path (GLD) and localizer (LOC) signals, respectively. These deviations are measured with respect to the receiver location on the aircraft near the cockpit that differs from the main landing gear position by $\delta x_{\mathrm{GLD}} \approx 28\,\mathrm{m}$, $\delta z_{\mathrm{GLD}} \approx -5\,\mathrm{m}$, and $\delta x_{\mathrm{LOC}} \approx 30\,\mathrm{m}$ for the benchmark aircraft. For large heading and pitch angles that occur during approach in crosswind, the difference cannot be ignored and the signals are corrected in order to keep the landing gear, rather than the receiver, on the glide path. Further, high frequency noise needs to be suppressed. This is achieved with complementary filters (e. g. Brockhaus et al., 2013) to ensure minor phase loss by augmenting the signals with surrogate measurements of their respective derivatives $\frac{\mathrm{d}}{\mathrm{d}t}\Delta z \approx V_z$ and $\frac{\mathrm{d}}{\mathrm{d}t}\Delta y \approx V_{\mathrm{g}} \sin\chi$. Thus, the geometrically corrected and filtered deviations are

$$\Delta\hat{z} = \frac{\omega_z}{s+\omega_z}\left((1-\delta x_{\mathrm{GLD}} \sin\Theta)\,\Delta z + \delta z_{\mathrm{GLD}} + \frac{V_z}{\omega_z}\right), \quad (2)$$

$$\Delta\hat{y} = \frac{\omega_y}{s+\omega_y}\left((1-\delta x_{\mathrm{LOC}} \sin\Psi)\,\Delta y + \frac{V_{\mathrm{g}} \sin\chi}{\omega_y}\right). \quad (3)$$

The filter bandwidths are set to $\omega_z = 2\,\mathrm{rad/s}$ and $\omega_y = 0.3\,\mathrm{rad/s}$ based on simulations.

The sink rate over ground is different from the inertial (barometric) sink rate, if the terrain is uneven. This becomes important during flare over sloped runways, as the objective is to touch down with a specified velocity *relative to the ground* (cf. Lambregts, 1982). Filtering the radar altitude H_{LG} by an approximate differentiation

filter with time constant $^1/_{15}$ s yields a sufficiently accurate estimate of the landing gear's sink rate over ground and still yields acceptable sensitivity to measurement noise. The feedback signal used during flare is thus

$$\hat{V}_z = \frac{15\,s}{s+15}\,H_{\mathrm{LG}}. \tag{4}$$

3. MIXED SENSITIVITY LOOPSHAPING DESIGN

Many properties of feedback control systems can be inferred from sensitivity functions, e. g. disturbance attenuation levels, tracking capabilities, the frequency range of control activity, and robustness. The fundamental closed-loop transfer functions of a multivariable unity feedback loop with plant model P, disturbance model P_d, and compensator C are (output) sensitivity $S = (I + P\,C)^{-1}$, control sensitivity $C\,S$, disturbance sensitivity $S\,P_d$, and input sensitivity $S_{\mathrm{i}} = (I + C\,P)^{-1}$. Mixed sensitivity loopshaping (e. g. Zhou et al., 1995; Skogestad and Postlethwaite, 2005) shapes these sensitivity functions through a weighted H_∞-norm optimization problem. The requirements are formulated through weighting filters, e. g. W_e and W_u in (5), that impose a desired shape such as low sensitivity at low frequencies. It is further possible to directly synthesize two-degrees-of-freedom controllers to improve transient behavior in response to a reference signal y_{ref}. Such a controller consists of feedback (C) and feedforward (C_{FF}) compensator, i. e., the control signal is $u = C_{\mathrm{FF}}\,y_{\mathrm{ref}} - C\,y$. The following generalized plant $G(C, C_{\mathrm{FF}})$ is used to specify the requirements:

$$G(C, C_{\mathrm{FF}}) = \begin{bmatrix} W_e & 0 \\ 0 & W_u \end{bmatrix} \begin{bmatrix} S\,P_d & S & I - S\,P\,C_{\mathrm{FF}} \\ C\,S\,P_d & C\,S & S_{\mathrm{i}}\,C_{\mathrm{FF}} \end{bmatrix}. \tag{5}$$

The controller is found from the optimization problem

$$\min_{C, C_{\mathrm{FF}}} \bar{\gamma} \text{ subject to } \|G\| < \bar{\gamma}, \tag{6}$$

for which standard numerical tools exist, e. g. `hinfsyn` in Matlab's Robust Control toolbox. Standard choices for W_e are filters with approximately integral behavior up to the desired bandwidth ω_b and a gain of 0.5 beyond that frequency. The rationale is to decrease sensitivity and disturbance sensitivity up to ω_b and to limit sensitivity degradation beyond that frequency to no more than a factor of two. The weight W_u is unity up to the available bandwidth ω_a for control and approximates a differentiator beyond that frequency to restrict control authority.

Sensitivity functions depend on the units of inputs and outputs of the plant, which necessitates scaling as suggested, e. g., in Skogestad and Postlethwaite (2005). Specifically, the diagonal matrices D_e of maximum allowable errors, D_u of maximum allowable inputs and D_d of maximum expected disturbances are used in this paper. The sensitivity functions of a closed loop with scaled models $\tilde{P} = D_e^{-1}\,P\,D_u$ and $\tilde{P}_d = D_e^{-1}\,P_d\,D_d$, and controller $\tilde{C}$ are related to those of the actual closed loop with controller $C = D_u\,\tilde{C}\,D_e^{-1}$ by

$$\begin{aligned} &\tilde{S} = D_e^{-1} S D_e,\ \tilde{S}_{\mathrm{i}} = D_u^{-1} S_{\mathrm{i}} D_u,\ \tilde{C}\,\tilde{S} = D_u^{-1} C S D_e \\ &\tilde{S}\,\tilde{P}_d = D_e^{-1} S P_d D_d, \quad \tilde{C}\,\tilde{S}\,\tilde{P}_d = D_u^{-1} C S P_d D_d. \end{aligned} \tag{7}$$

Scalings are thus important design parameters with a clear physical interpretation, e. g., D_u can be decreased to lower control activity (through $C\,S$) or D_d can be increased to emphasize disturbance rejection (through $S\,P_d$).

4. CONTROL DESIGN DETAILS

The design is based on a set of linear models obtained from linearization of the nonlinear aircraft model in quasi-steady approach, i. e., for constant sink rate, wings-level straight flight. This means that longitudinal and lateral directional dynamics are decoupled in the design. A disturbance model that represents wind inputs in all three directions is also included. The variety of possible load cases is considered in a grid of total mass between 120 t and 180 t in steps of 20 t and center-of-mass locations between 15 % and 40 % in steps of 5 %. The model with a mass of 150 t and a center-of-mass location of 20 % is used for design, with evaluations performed on all 24 models.

Wherever possible, simple single-loop controllers (PI and PD) that are easy to tune by means of classical loopshaping (e. g. Horowitz, 1963; Doyle et al., 1990) through Matlab's graphical user interface `sisotool` are used. Controllers that are designed in this way are colored blue in Fig. 1. Simple controllers further allow the use of conditional integration to prevent integrator wind-up in case of saturation. That is, the difference between commanded and applied control signal $\tilde{u} = u - \mathrm{sat}(u)$ is compared to the error and the integrator input is zeroed if both have the same sign. This compensation is implemented for all PI controllers, as control surface saturation needs to be expected during gusts where large amplitudes are required to actively mitigate disturbances. H_∞ controllers, colored red in Fig. 1, are used for lateral-directional and sink rate control. The choice of bandwidths for the weighting filters W_e and W_u are motivated by the discussion in Section 2 and tuning is performed by adjusting the scalings to trade off control effort versus performance in a very intuitive way. The Riccati-based robust anti-windup method of Sofrony et al. (2007) is used to avoid instability of the lateral-directional multivariable control loop in case of actuator saturation. It is based on representing the saturation as a disturbance that perturbs the linear model. The anti-windup compensator is synthesized such that this disturbance on the nominal model is minimized and only depends on the open-loop model and a single design parameter. The main advantages of the method are that it is independent of the controller and that it requires little to no tuning. Controllers are designed in continuous time domain and discretized for implementation through Tustin approximation with a sampling time of 0.05 s.

4.1 Autothrottle

The low engine bandwidth makes it impossible to counteract turbulence through throttle. A longitudinal model (u, w, q, Θ, and engine dynamics) is used and a PI controller $\delta_{\mathrm{th}} = 0.019\,(\frac{1}{s} + 15)\,(V_{\mathrm{ref}} - V_{\mathrm{cas}})$ is designed to achieve a closed-loop bandwidth of 0.25 rad/s, sufficient to maintain airspeed in case of changing average wind conditions.

4.2 Pitch Rate Control

A short period model (w, q, and actuator dynamics) is used and a PI controller $\delta_{\mathrm{e}} = -15\,(\frac{1}{s} + 0.71)\,(q_{\mathrm{ref}} - q) + 1.5\,q_{\mathrm{ref}}$ is designed to achieve a closed-loop bandwidth of 6 rad/s. The feedforward gain is added to avoid overshoot in response to command signals.

4.3 Sink Rate Tracker

A model of the short period dynamics (w, q, Θ), augmented with the previously designed pitch tracker, is used to design the sink rate loop. As a consequence of integral control on q, the design model already has integral behavior. The non-minimum phase zero at around 2.5 rad/s, associated with the acceleration response, imposes a hard limitation on the achievable bandwidth and severely complicates the design. As a consequence, mixed sensitivity loopshaping is used, which also has the added benefit of directly providing a feedforward controller. The desired bandwidth for sensitivity reduction is set to $\omega_b = 1.5\,\mathrm{rad/s}$ and the available bandwidth is set to $\omega_a = 3\,\mathrm{rad/s}$. Facing a single-input-single-output design problem, D_e is fixed to 1 as it could be absorbed in the other scalings, see (7). Maximum expected disturbances through wind gusts in x and z direction are set to $D_d = 2\,\mathrm{m/s}$. The scaling for the control signal, i. e. the maximum allowable pitch rate command, is tuned to $D_u = 0.03\,\mathrm{rad/s}$. The frequency response of the resulting sensitivity functions is shown in Fig. 2. The desired sensitivity reduction could not be achieved completely, but sensitivity is reduced up to 0.7 rad/s, sufficient to clearly improve disturbance rejection in the frequency range of gust disturbances (Fig. 2b). The tracking bandwidth (represented by SPC_{FF}) on the other hand indeed equals 1.5 rad/s (Fig. 2a), such that the design is considered successful.

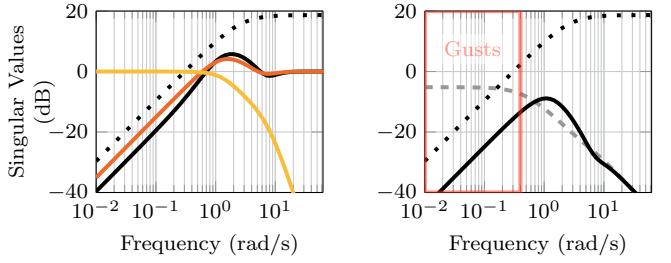

(a) S (—), $1 - SPC_{\mathrm{FF}}$ (—), $\bar{\gamma} W_e^{-1}$ (····), SPC_{FF} (—). (b) P_d (- - -), SP_d (—), $\bar{\gamma} W_e^{-1}$ (····).

Fig. 2. H_∞-design of sink rate control loop.

4.4 Lateral-Directional Control

A model of the longitudinal-directional dynamics (v, p, r, ϕ and actuator dynamics) is used to design the controller. The desired bandwidths for sensitivity reduction are set to $\omega_b = 0.5\,\mathrm{rad/s}$ for n_y and $\omega_b = 1.5\,\mathrm{rad/s}$ for Φ. The available actuator bandwidths are set to $\omega_a = 8\,\mathrm{rad/s}$ for the aileron and $\omega_a = 2.5\,\mathrm{rad/s}$ for the rudder. To achieve little cross coupling and well-damped responses, the maximum allowable errors D_e are selected as $0.1\,\mathrm{m/s^2}$ for n_y, 1° for Φ, and 1°/s for p and r. The maximum magnitude for lateral gust disturbances is selected as 5 m/s to emphasize disturbance rejection. Finally, the scalings for maximum control signals are tuned to 45° aileron and 30° rudder to remain inside the actuator limits. Figure 3 shows the frequency response of the resulting sensitivity functions. The desired sensitivity reduction is almost achieved and the feedforward part of the controller clearly improves decoupling (Fig. 3a). Disturbance rejection is also improved and the dutch roll mode is damped out (Fig. 3b).

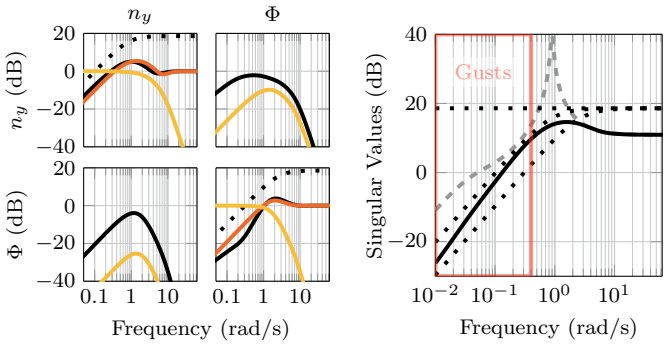

(a) S (—), $I - SPC_{\mathrm{FF}}$ (—), $\bar{\gamma} W_e^{-1}$ (····), SPC_{FF} (—). (b) P_d (- - -), SP_d (—), $\bar{\gamma} W_e^{-1}$ (····).

Fig. 3. H_∞-design of lateral-directional control loop.

4.5 Glide Path Tracking

The transfer function from V_z to Δz closely resembles an integrator in the frequency range of interest. Hence, a proportional controller $V_{z,\mathrm{ref}} = 0.2\,\Delta\hat{z}$ is selected to achieve a bandwidth of 0.2 rad/s. To ensure safe operation, we further limit the output of the loop to sink rate commands that deviate ±3 m/s from the trim value. The transfer function from Φ to Δy approximately equals a double integrator in the relevant frequency range. Thus, phase lead is required to stabilize the loop and a PD controller is designed to achieve a bandwidth of 0.6 rad/s. Differentiation is not actually performed, but instead the lateral velocity estimate $\frac{\mathrm{d}}{\mathrm{d}t}\Delta y \approx V_{\mathrm{g}} \sin\chi$ is used for feedback. The controller is $\Phi_{\mathrm{ref}} = 0.0035\,\Delta\hat{y} + 0.07\,V_{\mathrm{g}} \sin\chi$ and the commanded bank angle is limited to ±30° to ensure safe operation.

4.6 Flare

Flare is engaged at a fixed altitude of 13 m above ground and the autothrottle is deactivated. For an aircraft on the glide path, this is low enough to be over the runway in most situations (cf. Lambregts, 1982). Hence, a sloped runway can immediately be detected from the differentiated radar altitude (4). Ideally, the height should follow an exponentially decaying trajectory $H(t) = H_0 \mathrm{e}^{-t/\tau} + H_{\mathrm{bias}}$. This is achieved when $\dot{H} = -V_z = -1/\tau H_0$ and hence a feedback loop from radar altitude to sink rate reference is closed with $V_{z,\mathrm{ref}} = 1/\tau\,(H + H_{\mathrm{bias}})$. The constant H_{bias} is calculated such that the sink rate at flare initialization equals the sink rate during approach, i. e.,

$$H_{\mathrm{bias}} = \tau\, V_{z,\mathrm{Approach}} - H_{\mathrm{Flare}}\,. \tag{8}$$

The time constant is calculated as

$$\tau = H_{\mathrm{Flare}}/(V_{z,\mathrm{Approach}} - V_{z,\mathrm{Touchdown}}) \tag{9}$$

to result in a touchdown velocity $V_{z,\mathrm{Touchdown}} = 0.5\,\mathrm{m/s}$ (1.6 ft/s). The sink rate $V_{z,\mathrm{Approach}}$ depends on wind and the mass of the aircraft. Thus, H_{bias} and τ are calculated online, based on the measured sink rate. This leads to a "variable tau" control law as proposed by Lambregts and Creedon (1980). To mitigate the influence of gusts on the calculation, the sink rate is low-pass filtered with a time constant of 30 s. Further, the difference between the inertial sink rate and the sink rate over ground is subtracted. The latter is calculated through the much faster filter (4), such that the requirements for a sloped runway are taken into account. Both H_{bias} and τ are frozen

once the flare is engaged. The time constant turns out to be between 4–8 s in most cases, which satisfies the bandwidth constraint of 0.6 rad/s discussed in Section 2.

4.7 Decrab

Decrab is activated at an altitude of 5 m above ground. A proportional controller $n_{y,\mathrm{ref}} = 5\,(\Psi - \chi)$ is selected, corresponding to a control loop bandwidth of 0.5 rad/s. Bank angle is still controlled through the glide path tracker during decrab to keep the flight path aligned with the centerline, but the limits on bank angle commands are tightened to ± 10° to avoid the risk of touching down with the wing tips first. The reference for Φ is set to zero shortly before touchdown at an altitude of 2 m above ground in order to completely level the wings.

5. DESIGN VERIFICATION

The autolanding system is verified on the nonlinear aircraft model [1] in turbulent wind according to the challenge's evaluation criteria, i. e., the risk of short landing, long landing, hard landing, decentered landing, landing with steep bank angle, and landing with steep wheel sideslip angle, see Biannic and Boada-Bauxell (2016). Figure 4a shows the final phase of a landing in non-turbulent crosswind to illustrate these criteria. The upper left plot depicts the main landing gear's altitude H_{LG} above ground. The point for evaluating the *short landing* criterion is the altitude 60 m after the runway threshold and is marked with a square. The altitudes for flare, decrab, and wings level initialization are visualized by gray lines. The touchdown point evaluated for the *long landing* criterion is marked with a diamond. The exponential flare trajectory is clearly visible. The upper right plot shows the sink rate above ground. The touchdown speed for the *hard landing* criterion is marked with a triangle and the maximum value of 3.05 m/s (10 ft/s) is indicated by the arrow on the right. The aircraft touches down gently, with a velocity close to the specified value of 0.5 m/s. The lower left plot shows a view on the runway from above with the centerline highlighted in green. The trajectory of the aircraft closely follows the centerline all the way through flare and also decrab. It starts to deviate only after the wings level command is given, which is expected as position is no longer controlled from this point on. The touchdown point determines the *decentered landing* criterion and is marked with a cross. Arrows on the right illustrate the maximum admissible deviation of ±15 m from the centerline. Bank angle and wheel sideslip are shown in the lower right plot and the values at touchdown that determine the *steep bank angle* and *steep wheel sideslip* critera are marked by circles. The aircraft approaches crabbed with a heading of about 23° and zero bank angle. Once decrab is initiated, heading is quickly reduced to less than 10° with only minor effect on the bank angle. The admissible range is again marked by arrows on the right. A simulation with strong turbulent wind and a sloped runway is shown in Figure 4b for comparison. A short upwards motion is apparent after the wings level command is issued, slightly delaying touchdown. In addition to the

[1] CALC package version 6, 24-Oct-2016, available from `http://w3.onera.fr/smac/?q=aircraftModel`

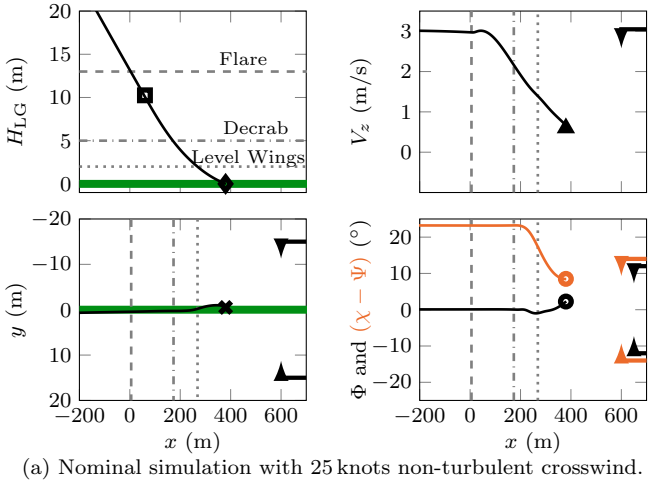

(a) Nominal simulation with 25 knots non-turbulent crosswind.

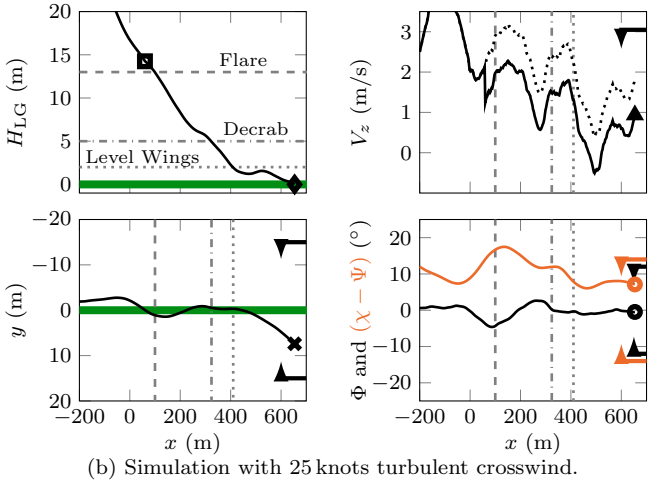

(b) Simulation with 25 knots turbulent crosswind.

Fig. 4. Nonlinear simulation of of crosswind landing with marks for evaluation criteria: H_{60} (■), X_{T} (◆), $V_{z,\mathrm{T}}$ (▲), Y_{T} (✖), Φ_{T} (●), and β_{T} (●).

sink rate over ground, the upper right plot also shows the inertial sink rate in dashed. They differ due to a downsloped runway, leading to a discontinuity in the model. The flare maneuver clearly reduces the sink rate, although strong gust disturbances are visible in the response. The touchdown velocity is again close to the desired value. The aircraft still very tightly tracks the centerline up to the wings level command and the final deviation is well within the admissible range. Heading and bank are also well controlled and the decrab maneuver induces no visible roll disturbance. Qualitatively, all of these results agree with the nominal simulation, confirming the controller's ability to handle turbulent wind conditions.

The six criteria are next evaluated in Monte Carlo simulations to verify robustness. The maximum crosswind speed is first set to $W_y = 25$ knots and 2000 simulations with random parameters, distributed according to Table 1, are performed to determine the average risk dispersion. In a second step, 2000 simulation trials are performed to determine the limit risk dispersion with crosswind fixed to W_y and all other parameters following Table 1. These two steps are repeated in a second evaluation campaign for $W_y = 30$ knots. Figure 5 shows the resulting risk dispersions as cumulative distribution functions for each of the six evaluation criteria. The challenge's requirements are

Table 1. Monte Carlo Parameters for Verification.

Parameter	distribution*	min	max
Longitudinal wind (knots)	$\mathcal{N}(7.5, 7.5)$	10 tail	30 head
Lateral wind (knots)	$\mathcal{N}(0, 7)$	W_y left	W_y right
Mass (t)	uniform	120	180
Center of mass (%)	uniform	15	41
Runway altitute (ft)	specific**	-1000	9200
Temperature (°C)	uniform	-69	40
Runway slope (%)	$\mathcal{N}(0, 0.4)$	-2	2
Glide slope (°)	$\mathcal{N}(-3, 0.075)$	-2.85	-3.15
Localizer bias (μA)	$\mathcal{N}(0, 2.5)$	-5	5

*$\mathcal{N}(\mu,\sigma)$: normal distribution with mean μ and standard deviation σ.
**see Biannic and Boada-Bauxell (2016) for the distribution.

illustrated by the yellow and red areas. The distribution function has to be completely outside of these areas for average risk. For limit risk, it is allowed to penetrate the yellow areas, but must remain outside the red areas. The *decentered landing* criterion, for example, requires the probability for a lateral deviation of greater than 15 m from the centerline at touchdown to be less than 10^{-6} for average risk and less than 10^{-5} for limit risk. All criteria are satisfied for 25 knots maximum crosswind by our design. The margin for the average risk dispersion is large and in fact, the present design also easily satisfies the average risk requirements for 30 knots maximum wind speed. The limiting factors are the *hard landing* and *wheel sideslip* criteria, for whom the limit risk requirements are violated at 30 knots wind speed. *Hard landing* can be attributed to insufficiently tight sink rate control during flare. Improving this is however not easy, as the non-minimum phase zero imposes a hard constraint on the achievable bandwidth of the control loop and strong gusts can cause rate limit saturation in the elevator actuator. Similarly, *wheel sideslip* is related to insufficient yaw control during decrab that appears to be restricted by aileron saturation (to counteract the roll moment induced by decrabbing).

6. CONCLUSION

A comprehensive autopilot design for crosswind landings was presented. The selection of a suitable cascaded control architecture, necessary signal modifications, and the design of all required control loops were detailed. The design parameters have a clear relation to the design requirements so that little tuning effort was required. The control system was evaluated in nonlinear Monte Carlo simulations and shown to successfully land the aircraft in turbulent crosswind of up to 25 knots.

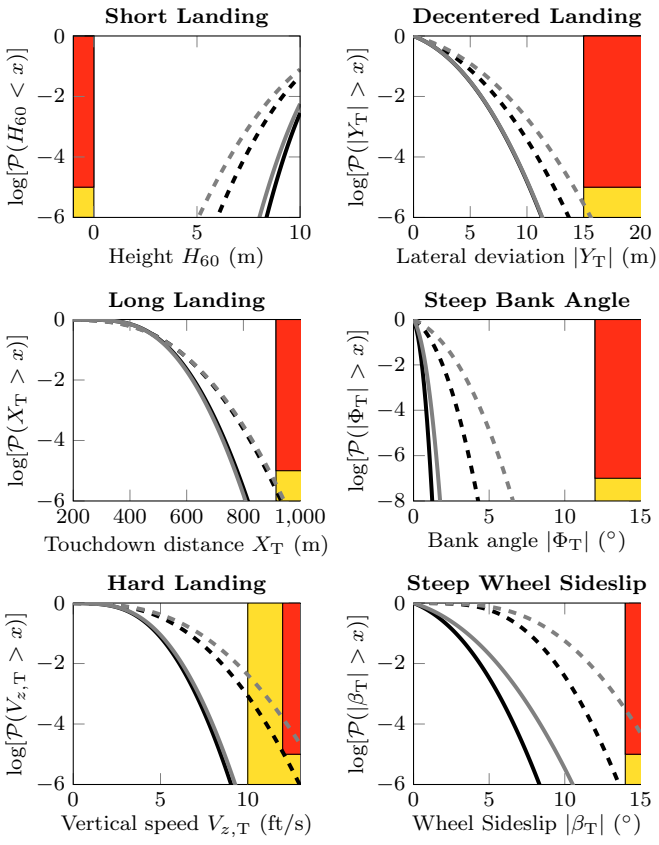

Fig. 5. Risk dispersions for 25 (average —/limit - - -) and 30 knots (—/- - -) maximum crosswind, each obtained through 2000 Monte Carlo Simulations.

REFERENCES

Biannic, J.M. and Boada-Bauxell, J. (2016). A civilian aircraft landing challenge. On-line available from the aerospace benchmark section of the SMAC Toolbox. URL `http://w3.onera.fr/smac/`.

Biannic, J. and Roos, C. (2015). Flare control law design via multi-channel H_∞ synthesis: Illustration on a freely available nonlinear aircraft benchmark. In *American Control Conference*, 1303–1308.

Brockhaus, R., Alles, W., and Luckner, R. (2013). *Flugregelung*. Springer, Berlin.

de Bruin, A. and Jones, T. (2016). Accurate autonomous landing of a fixed-wing unmanned aircraft under cross-wind conditions. In *20th IFAC Symposium on Automatic Control in Aerospace*.

Doyle, J., Francis, B., and Tannenbaum, A. (1990). *Feedback Control Theory*. Macmillan Publishing Co.

Holley, W. and Bryson, A. (1977). Wind modeling and lateral control for automatic landing. *Journal of Spacecraft and Rockets*, 14(2), 65–72.

Horowitz, I. (1963). *Synthesis of Feedback Systems*. Academic Press, New York.

Lambregts, A. (1982). Avoiding the pitfalls in automatic landing control system design. In *AIAA Guidance and Control Conference*.

Lambregts, A. and Creedon, J. (1980). Development and flight evaluation of automatic flare laws with improved touchdown dispersion. In *AIAA Guidance and Control Conference*. Paper 80-1757.

Looye, G., Joos, H.D., and Willemsen, D. (2001). Application of an optimisation-based design process for robust autoland control laws. In *AIAA Guidance, Navigation, and Control Conference*.

McRuer, D., Ashkenas, I., and Graham, D. (1973). *Aircraft Dynamics and Automatic Control*. Princeton University Press, Princeton, NJ.

Skogestad, S. and Postlethwaite, I. (2005). *Multivariable Feedback Control*. Prentice Hall, Upper Saddle River, NJ.

Sofrony, J., Turner, M.C., and Postlethwaite, I. (2007). Anti-windup synthesis using Riccati equations. *International Journal of Control*, 80(1), 112–128.

Zhou, K., Doyle, J., and Glover, K. (1995). *Robust and Optimal Control*. Prentice Hall, Upper Saddle River, NJ.